European Journal of Medicinal Chemistry 207 (2020) 112836

Contents lists available at ScienceDirect

European Journal of Medicinal Chemistry

journal homepage: http://www.elsevier.com/locate/ejmech

Research paper

An electrophilic warhead library for mapping the reactivity and accessibility of tractable cysteines in protein kinases

László Petri [a], Attila Egyed [a], Dávid Bajusz [a], Tímea Imre [b], Anasztázia Hetényi [c], Tamás Martinek [c], Péter Ábrányi-Balogh [a], György M. Keserű [a, *]

[a] Medicinal Chemistry Research Group, Research Centre for Natural Sciences, Magyar Tudósok Krt 2, H-1117, Budapest, Hungary
[b] MS Metabolomics Research Group, Research Centre for Natural Sciences, Magyar Tudósok Krt 2, H-1117, Budapest, Hungary
[c] Department of Medicinal Chemistry, University of Szeged, Dóm Tér 8, H-6720, Szeged, Hungary

ARTICLE INFO

Article history:
Received 11 November 2019
Received in revised form
3 September 2020
Accepted 7 September 2020
Available online 12 September 2020

Keywords:
Warhead selection
Kinase cysteome profiling
Targeted covalent inhibitors
Small-molecule kinase inhibitors
JAK3
MELK

ABSTRACT

Targeted covalent inhibitors represent a viable strategy to block protein kinases involved in different disease pathologies. Although a number of computational protocols have been published for identifying druggable cysteines, experimental approaches are limited for mapping the reactivity and accessibility of these residues. Here, we present a ligand based approach using a toolbox of fragment-sized molecules with identical scaffold but equipped with diverse covalent warheads. Our library represents a unique opportunity for the efficient integration of warhead-optimization and target-validation into the covalent drug development process. Screening this probe kit against multiple kinases could experimentally characterize the accessibility and reactivity of the targeted cysteines and helped to identify suitable warheads for designed covalent inhibitors. The usefulness of this approach has been confirmed retrospectively on Janus kinase 3 (JAK3). Furthermore, representing a prospective validation, we identified Maternal embryonic leucine zipper kinase (MELK), as a tractable covalent target. Covalently labelling and biochemical inhibition of MELK would suggest an alternative covalent strategy for MELK inhibitor programs.

1. Introduction

Medicinal chemistry programs investigating covalent inhibitors have come of age in the last decade [1,2]. Intensive targeted covalent inhibitor (TCI) development in oncology has resulted in *afatinib* (Gilotrif®) [3], an EGFR inhibitor that suppress the growth and proliferation of tumor cells. It was a true milestone in cancer therapy, and became the first FDA-approved covalent small-molecule kinase inhibitor in 2013. Covalent small-molecule kinase inhibitors represent a target-specific subtype of TCIs. Kinases are one of the major classes of signaling proteins that trigger a variety of biochemical processes (e.g. modulating enzyme activity, changing protein conformation, increasing or decreasing stability, activating protein functions) through their phosphorylation [4]. Kinase signaling pathways are involved in various diseases, like immune disorders, cardiovascular and metabolic diseases and most importantly a large number of different cancers [5,6]. Consequently, there has been a high demand for the design and development of kinase inhibitors, particularly in the field of oncology [7]. Over the past few years, approximately 40 kinases have been pursued as potential targets [8], but only few targeted covalent inhibitors have received FDA approval: e.g. *afatinib* [3] (Gilotrif®), *osimertinib* [9] (Tagrisso®), *neratinib* [10] (Nerlynx®) and *dacomitinib* [11] (Vizimpro®) targeting EGFR, or *acalabrutinib* [12] (Calquence®) and *ibrutinib* [13] (Imbruvica®) targeting BTK.

TCI molecules consist of two main parts: in addition to the noncovalent drug-like scaffold, they are equipped with an appropriate electrophilic warhead [14–18]. In addition to the optimization of noncovalent interactions, rational design of the warhead moiety is of utmost importance [19,20]. The different location and surroundings of the targeted cysteine influence its reactivity and accessibility through changes in the protonation state, the spatial arrangement of the reacting groups, the geometries of the transition states, the intermediates and the product of the covalent bond-forming reaction [21]. These factors distinguish between the labeling properties of the cysteine residues. In fact, recent proteomic studies have suggested that cysteine reactivity might be

* Corresponding author.
E-mail address: keseru.gyorgy@ttk.hu (G.M. Keserű).

https://doi.org/10.1016/j.ejmech.2020.112836

remarkably diverse in distinct proteins [22]. Thus, selecting the appropriate warhead first requires assessment of the reactivity and accessibility of the targeted cysteine [23]. The available experimental methodologies to evaluate the tractability of cysteines are using activity-based protein profiling (ABPP) [22,24,25] These are all proteomic-level screening techniques performed on living cells and require a powerful MS/MS platform. Even with this high-end instrumentation, other factors, such as the diversity of targets, influence of unknown cellular proteins, and low abundance of the modified protein make the detection of protein adducts in a complex matrix challenging. The only alternatives are computational techniques that have been used for the identification and characterization of reactive cysteines [26–32]. Compilation of targetable cysteines across the human kinome has inspired various research groups, and attempts have been carried out using X-ray based [33], sequence-based [34] and interaction fingerprint-based methodologies [27]. In addition to their position and accessibility, the protonation state of the cysteine thiol has a major influence on its reactivity. Recent articles evaluating cysteine pK_a values include a statistical analysis by Zhang et al. [29] and a sophisticated computational study by Awoonor-Williams and Rowley [26]. These studies suggest that the targeted cysteines should have a relatively low pK_a value, so that the more nucleophilic thiolate form will dominate [35].

Here we introduce a ligand-based technique for mapping cysteine reactivity and accessibility by screening a set of covalent fragments with diverse reactivity. Furthermore, the best performing warheads might serve as a viable starting point for fragment-based optimization aiming to develop targeted covalent inhibitors [36,37]. Although several comparative studies have been published on warhead reactivity [38–40], our library of warheads equipped to the same scaffold represents a unique opportunity for the efficient integration of warhead optimization into the covalent drug development process. In our preliminary study we found that a smaller proof-of-concept library covered a wide range of reactivity in surrogate assays [41]. Screening of the extended library described herein against protein kinases provides experimental reactivity and accessibility data of the targeted cysteines.

2. Results and discussion

2.1. Design and characterization of the covalent fragment library

A ligand-based cysteine mapping technique requires a carefully designed toolbox of covalent probes. Thus, first we intended to compile a preconceived set of fragments suitable for the assessment of the targeted cysteines *via* protein-level biochemical assays. Focusing on the covalent action we kept the noncovalent moiety small and apolar to minimize the noncovalent interaction contribution to fragment binding [42]. Thus, we chose the 3,5-bis(trifluoromethyl)phenyl scaffold, which showed no interference with any of the assay components, was stable in the assay conditions, provided easy detection by HPLC-MS and ^{19}F NMR, and furthermore, the electron withdrawing character of the trifluoromethyl substituents could activate the electrophilic center of the warheads. In total, we selected 24 covalent fragments (**1**-**24**) (Fig. 1) representing different levels of size and complexity. In addition, the flexibility of the warheads had also a large variety depending on the double or triple bonds, the direct C–C connection or binding through an amide bond or a methylene group to the aromatic ring. The library members or their corresponding intermediates were obtained from commercial sources or by synthesis (for the synthesis details see Supplementary Methods).

Assessing the electrophilic character of the probes, we calculated the local electrophilicity index [43]. These data showed that the library covers a wide range of theoretical electrophilicity (local EPI values of −0.148 for the least and of 0.581 for the most electrophilic probe). For the experimental confirmation, we have tested the probe library in a GSH-reactivity assay [39,44] (Supplementary Table S1). Nine fragments showed weak reactivity ($k_{GSH} < 0.01\ h^{-1}$ for **7**, **8**, **13**–**16**, **18**, **19** and **24**), seven fragments had moderate reactivity ($0.01 < k_{GSH} < 0.5\ h^{-1}$ for **1**, **3**, **9**, **17**, **21**, **22**, **23**) and additional seven fragments (**2**, **5**, **6**, **10**, **11**, **12**, **20**) were found to be highly reactive in the GSH assay. There were some warheads that showed similar reactivities (e.g. **8**, **14**, **18** and **1**, **17**); however, their labeling mechanisms are quite different and therefore either might be preferred at certain cysteine targets [21]. The cysteine selectivity of the applied covalent fragments was confirmed in our recently introduced oligopeptide assay [44]. As cysteine reactivity can be highly influenced by its environment in a particular protein, the broad spectrum of chemical reactivities and labeling mechanisms might significantly support the mapping efficiency of the probe library. Thus, this specific covalent fragment library could be a useful chemical toolbox for experimental mapping of the reactivity and accessibility of targeted cysteines.

2.2. Mapping the reactivity of kinase cysteines

As differences in the active sites of kinases influence the reactivity and accessibility of the targeted cysteines, we proposed to map the cysteine reactivity profile of main kinase families. The target kinases were selected as therapeutically significant and already covalently targeted members of the kinase phylogenetic tree that provides good coverage of the human kinome based on their inferred evolutionary relationships (Fig. 2) [45].

Taking into account the availability of covalently tractable cysteine residues [27], four kinases were picked up from different branches. We selected BTK from the TK (tyrosine kinase) branch, ERK2 from the CMGC (containing the families CDK, MAPK, GSK3 and CLK) branch, RSK2 from the AGC (containing the families PKA, PKG and PKC) branch and MAP2K6 from the STE (yeast sterile 7-,11- and 20-homologous kinases) branch. Known covalent inhibitors of the selected kinases are summarized in Supplementary Information Table S2 according to their major warhead chemotypes. The mapping library (**1**–**24**) was screened on the four kinases. Kinase activity was assessed at a concentration of 100 μM of each fragment with the selected kinases (BTK, ERK2, RSK2, MAP2K6) after 60 min of incubation in duplicate. The results of the activity profiling are shown as radar plots in Fig. 3 (for detailed results, see Supplementary Table S3).

As expected, different targets showed different activity profile. Particularly, of the 24 covalent fragments, **5**, **6**, **12** and **23** displayed high activities (≥70%) across the whole panel, while consistently low inhibition values (<50%) were determined for **3**, **9**, **14**, **15**, **16**, **18** and **24**. The remaining thirteen fragments represent the discriminatory power of the various warhead chemistries among the kinases in the panel. Some have a clear preference for one of the kinases, such as **13** (RSK2) or **19** (BTK), while others display various patterns among the panel, such as **8** (RSK2) or **22** (active against all but ERK2). It has been observed that the intrinsic reactivity overcame the impact of the warhead size. For instance, the bulky maleimides (**5** and **6**), although they are among the largest warheads in this study, performed exceedingly on all investigated kinases. On the contrary, the **12** isothiocyanate, which is less influenced by steric factors, also performed remarkably well. In spite of these examples, the sterically least hindered warheads, such as the styrene (**13**), the acetylene (**14**) or the nitrile (**15**), but also the larger *Boc*-protected hydrazine (**16**) did not show significant inhibition of any of the kinases. However, the smallest warhead, fluorine (**22**) showed quite diverse reactivity profile, while the second smallest

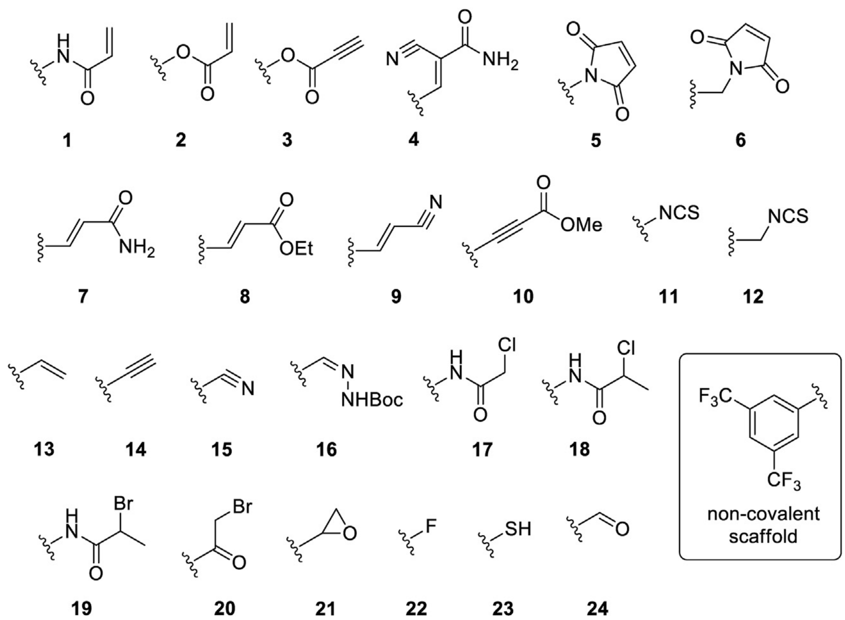

Fig. 1. Covalent fragment probes **1**–**24**.

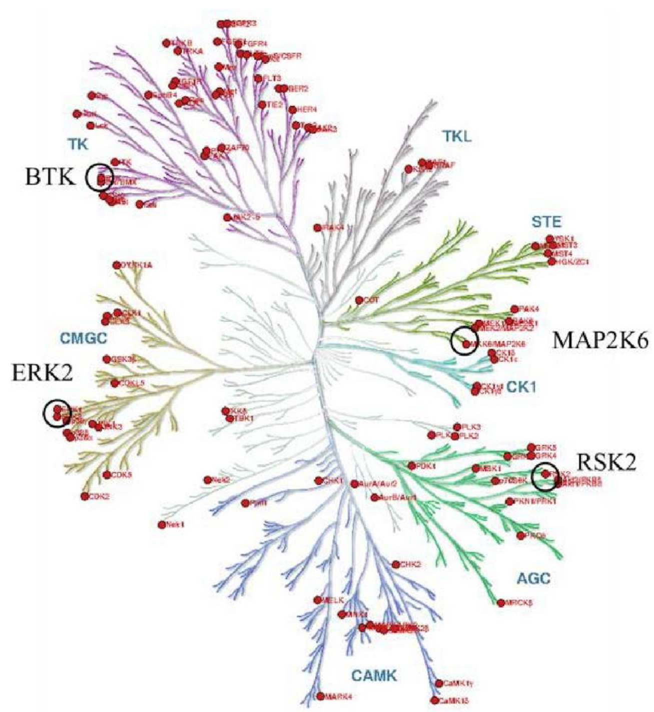

Fig. 2. Kinases that contain at least one targetable cysteine and are available for testing with the selected enzyme activity assay (Z′-LYTE, Life Technologies), indicated (with red dots) on the kinase phylogenetic tree. Black circles show kinases involved in the mapping. The figure was prepared with the Kinome Render program [46]. (For interpretation of the references to color in this figure legend, the reader is referred to the Web version of this article.)

warhead, thiol (**23**) resulted in high inhibition activity on all of the kinases. Moreover, it seems that the biological activity was mainly influenced by the warhead chemistry and the common scaffold provided low contribution to the inhibition potency. This is underlined by the comparison of the appropriate compounds: **1**, **5**, **14** and **24**. Compound **1** is equipped with a widely used warhead (acrylamide) that shows specific inhibition against BTK, while it has no significant biological activity on the other 3 kinase targets (ERK2, RSK2 and MAP2K6). This suggests that not only reactivity differences but selectivity issues can be addressed directly to the warhead chemistry. In addition, fragment **5** equipped with a highly reactive maleimide warhead – used extensively in protein labelling studies – inhibit all of the targets. Finally, fragments **14** and **24** carrying the acetylene and the aldehyde function, respectively, that have limited cysteine-reactivity [17,47] did not show significant inhibition against any of the targets, however it has the same scaffold as used for all the library members. We found that changing the chlorine to bromine in the warhead, however, leads to increased inhibition against BTK (39% with **16** → 94% with **17**), suggesting that small changes can influence the activity significantly while keeping the noncovalent core unchanged. It is important to note that different warhead chemistries represent various degrees of reactivity and different transition state/product geometries, while the location and the environment of the cysteines adds another layer of diversity that also influences the overall results.

2.3. Retrospective validation on JAK3

JAK3 was chosen as potential target for retrospective validation. Noteworthy, the active site of the JAK family is highly conserved, thus selectively achieving ATP-competitive inhibition is challenging. However, a non-conserved cysteine (Cys909) residue is located near the ATP binding site of JAK3, while no vulnerable nucleophilic residue can be found at the active sites of other JAK-subtypes. This unique feature makes JAK3 tractable and alluring for covalent inhibitor programs [48–52]. Sequence analysis (Supplementary Table S4) showed that BTK has the most similar active site to JAK3. As a first step of validation, we screened the mapping library against JAK3 and compared the reactivity profile to that of BTK (Fig. 4 and Supplementary Table S3). We found that the calculated reactivity and accessibility of the JAK3 active site cysteine (Supplementary Table S4) was by far the closest to BTK based on the calculated pK_a values and H-bond contributions, as well as the accessibility (solvent-exposed surface area, SASA) of the

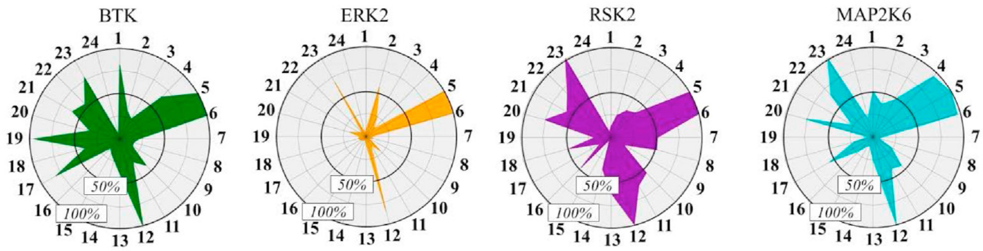

Fig. 3. Radar plots of the inhibitory activities of the covalent fragment library (**1**–**24**).

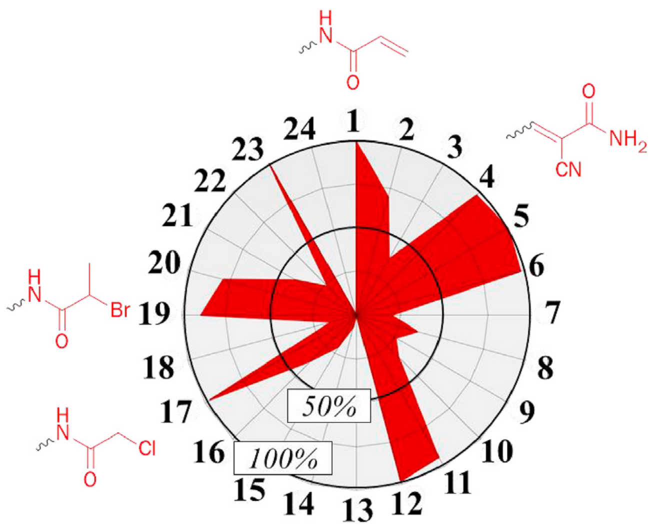

Fig. 4. Radar plot of the inhibitory activity of the covalent fragment library against JAK3 together with the warheads chosen for further analysis.

cysteines. Consequently, the results of ligand based cysteine reactivity mapping are in line with the sequential and structural similarity of the two kinases. Upon analyzing the inhibition profiles of JAK3 and BTK, after excluding the promiscuous warheads, we concluded that the warheads of probes **1**, **4**, **17** and **19** (acrylamide, cyano-acrylamide, chloroacetamide and 2-bromopropanamide, respectively) could provide the best affinity and selectivity for JAK3 compounds (Fig. 4). Covalent labeling of the Cys909 residue with the **1** and **17** probes was confirmed by MS/MS studies after digestion of the incubated protein samples (Supplementary Fig. S1).

Next, we challenged our warhead selection strategy by using the chosen warheads on a well-established hinge binder scaffold, 4-phenyl-pyrrolo[2,3-*d*]pyrimidine that is utilized by many kinase inhibitors [49,52–54]. This scaffold is providing a synthetically feasible option for warhead optimization. The synthesis of the compounds was carried out in two main steps starting with the preparation of the appropriate intermediates (**25**–**26**, Scheme 1a) directly prepared by the Suzuki coupling of 4-chloro-1*H*-pyrrolo[2,3-*d*]pyrimidine (**27**) and the properly substituted phenylboronic acid (**28**–**29**) [52]. Cyano-acrylamide **30** was derived from **25** aldehyde by Knoevenagel condensation [55] (Scheme 1b), while compounds **31** and **32** were synthesized from **26** amine by the corresponding acylation (Scheme 1c). In addition, to confirm the significant contribution of the covalent interaction to the inhibition, we decided to investigate **32** noncovalent control containing the same scaffold equipped with an acetamide functional group instead of an electrophilic warhead.

Introducing the selected warheads from fragments **1** and **17** led to known covalent JAK3 inhibitors **33** and **34** (Scheme 1d) having low nanomolar or even subnanomolar IC_{50} (0.77 and 1.02 nM, respectively) [54]. Notably, **33** acrylamide was confirmed to bind JAK3 ATP-site covalently through Cys909 [52]. The **30** cyano-acrylamide derived from fragment **4** showed some activity against MAP2K6 and RSK2 [56] (281 and 399 nM, respectively) but blocked JAK3 more effectively (IC_{50} = 55.9 nM). Finally, using the haloacetamide warhead of fragment **19** resulted in a novel covalent JAK3 inhibitor (**31**) with an IC_{50} = 10.6 nM (Scheme 1).

Using the most effective warheads identified by screening our probe library we confirmed that noncovalent interactions are not solely responsible for the selectivity and specificity of covalent inhibitors. Compounds **30,31,33** and **34** differ from **32** only in the presence of an electrophilic warhead suggesting that the covalent interaction contributes significantly to the observed activity (IC_{50} = 832 nM for **32** and 0.77–55.9 nM for **30**, **31**, **33**, **34**). Furthermore, introducing the selected warheads to a hinge binder scaffold, we successfully retrieved already known JAK3 inhibitors (**33** and **34**) and identified two additional compounds with low-nanomolar activity (**30** and **31**). Our results suggest that the mapping of active site cysteines in other kinase targets provides useful information on the reactivity and accessibility of the targeted residue and could help in finding the appropriate warheads for targeted covalent inhibitors.

2.4. Prospective validation on MELK

Promising results obtained during the retrospective validation of the cysteine mapping protocol prompted us to apply this strategy prospectively to identify other potential targets for covalent drug discovery programs. For this purpose, we chose MELK kinase which has recently been emerged as an active research target in various oncology-related indications [57–61]. Noteworthy, to the best of our knowledge, no validated covalent inhibitor for MELK has been disclosed yet. Therefore, we decided to analyze the tractability of MELK applying the ligand-based mapping technique presented herein. The activity profile is shown in Fig. 5a (for detailed results see Supplementary Table S3) that suggested three suitable warheads for covalent targeting of MELK including the **4** cyano-acrylamide, the **11** isothiocyanate and the **20** bromoacetophenone warheads. Motivated by the high fluorine content of the probes, covalent labelling was confirmed by ^{19}F NMR measurements (Fig. 5b). In fact, fragments have been incubated with the isolated MELK protein, and the change in the ^{19}F NMR shifts has been followed for 24 h. Comparing the spectra with the protein-free reference, probes **4**, **11** and **20** were proven to label covalently MELK (Supplementary Fig. S2) with the labelling efficiency of 97%, 30% and 60%, respectively. We have chosen the most potent warhead chemotype (particularly the cyano-acrylamide, **4**), and together with the general hinge binder scaffold, we tested the previously synthesized analogue (**30**) against MELK (Fig. 5c).

Measuring the activity on MELK we found that **30** is an effective inhibitor (IC_{50} = 25.5 nM, Fig. 5c), while the noncovalent control **32**

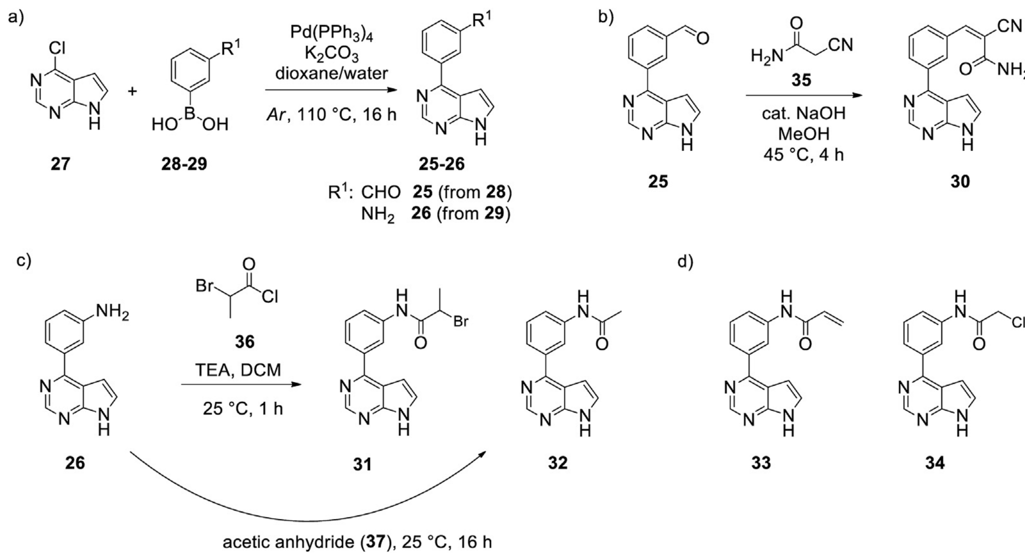

Scheme 1. Synthetic routes to the designed covalent JAK3 inhibitors: (a) Key intermediates **25**–**26** were prepared by Suzuki coupling; (b) synthesis of cyano-acrylamide **30**; and (c) synthesis of amides **31**–**32**. d) Covalent JAK3 inhibitors (**33**, **34**) retrieved retrospectively.

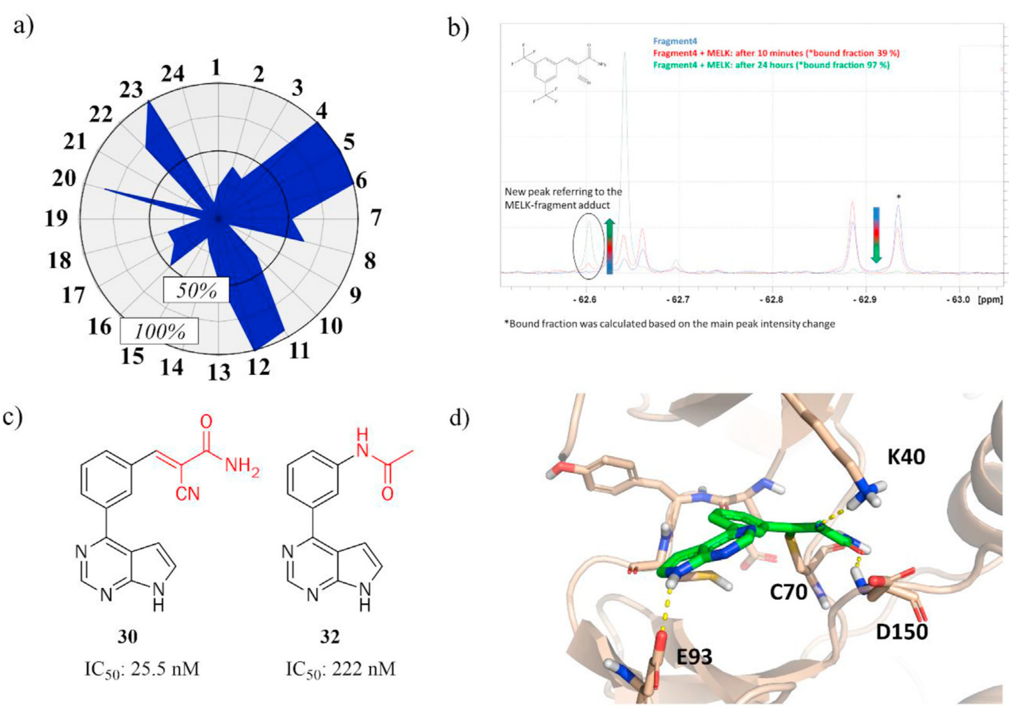

Fig. 5. a) Radar plot of the inhibitory activity of the covalent fragment library against MELK. b) Covalent binding of probe **4** confirmed by ^{19}F NMR. c) MELK inhibitory activity of compound **30** and its noncovalent control (**32**). d) Proposed binding mode of compound **30** at the ATP site of MELK.

resulted in a magnitude higher IC_{50} (222 nM, Fig. 5c). The order of magnitude difference between the IC_{50} data suggests the significant contribution of the covalent interaction. Although the exact site of labelling could not be identified by preliminary MS/MS experiments, computational analysis identified two tractable cysteines [27]. One of these residues are located in the hinge region at position Hinge-2 (Cys89), the other sits in the hydrophobic subpocket at position Beta-4-2 (Cys70). Covalent docking of **30** to the ATP site of MELK suggests the latter as the potential site of labelling (Fig. 5d).

3. Conclusion

Here we provided a novel and readily available ligand based alternative for the experimental characterization of tractable cysteines and target-specific selection of electrophilic warheads. We showed that screening a small library of electrophiles provides reactivity and accessibility information on targeted cysteines, which might be useful identifying tractable targets for covalent inhibition. Our approach selects proper warheads for noncovalent kinase inhibitor scaffolds turning them into covalent inhibitors. The approach has been first challenged in a retrospective validation with JAK3. Testing the probe library we selected suitable JAK3 warheads and then equipped these to a known hinge binder core fragment (4-phenyl-pyrrolo[2,3-*d*]pyrimidine). This design strategy resulted in four covalent inhibitors, two known compounds were retrieved and two further compounds were identified as novel covalent JAK3 inhibitors. The usefulness of our cysteine profiling strategy has been confirmed prospectively on MELK as a target. Screening the probe library suggested three potential warheads and their covalent binding was subsequently confirmed by ^{19}F NMR measurements. Using the most effective cyano-acrylamide warhead, we identified a novel covalent MELK inhibitor with low-nanomolar activity. Based on the success of both the retrospective and prospective application we suggest screening the probe library to evaluate the accessibility and reactivity of targeted cysteines in protein kinases and to select potential warheads for developing novel covalent inhibitors. The probe library is available in physical form from the authors upon request. Considering the significant efforts invested to discover new warhead chemotypes, we plan to include these new warheads in the next edition of the probe library.

4. Experimental section

4.1. Instruments

^{1}H NMR spectra were recorded in DMSO-d_6 or $CDCl_3$ solution at room temperature, on a Varian Unity Inova 500 spectrometer (500 MHz for ^{1}H NMR spectra), with the deuterium signal of the solvent as the lock and TMS as the internal standard. Chemical shifts (δ) and coupling constants (J) are given in ppm and Hz, respectively.

^{19}F NMR measurements were performed using a 500 MHz Bruker Avance NEO spectrometer equipped with a 5 mm Prodigy BBO probe with z-gradient at 298 K.

HPLC-MS measurements were performed using a Shimadzu LCMS-2020 device equipped with a Reprospher 100C18 (5 μm; 100 × 3mm) column and positive-negative double ion source (DUIS±) with a quadrupole MS analyzator in a range of 50−1000 *m/z*. Sample was eluted with gradient elution using eluent A (10 mM ammonium formate in water:acetonitrile 19:1) and eluent B (10 mM ammonium formate in water:acetonitrile 1:4). Flow rate was set to 1 ml/min. The initial condition was 0% B eluent, followed by a linear gradient to 100% B eluent by 1 min, from 1 to 3.5 min 100% B eluent was retained; and from 3.5 to 4.5 min back to initial condition with 5% B eluent and retained to 5 min. The column temperature was kept at room temperature and the injection volume was 10 μl. Purity of compounds was assessed by HPLC with UV detection at 215 nm; all tested compounds were >95% pure.

A Sciex 6500 QTRAP triple quadrupole − linear ion trap mass spectrometer, equipped with a Turbo V Source in electrospray mode (Sciex, CA, USA) and a PerkinElmer Series 200 micro LC system (Massachusetts, USA) consisting of binary pump and an autosampler was used for LC−MS/MS analysis. Data acquisition and processing were performed using Analyst software version 1.6.2 (AB Sciex Instruments, CA, USA). Chromatographic separation was achieved by Purospher STAR RP-18 endcapped (50 mm × 2,1 mm, 3 μm) LiChocart® 55-2 HPLC Cartridge. Sample was eluted with gradient elution using solvent A (0.1% formic acid in water) and solvent B (0.1% formic acid in acetonitrile). Flow rate was set to 0.5 ml/min. The initial condition was 5% B for 2 min, followed by a linear gradient to 95% B by 6 min, from 6 to 8 min 95% B was retained; and from 8 to 8.5 min back to initial condition with 5% eluent B and retained to 14.5 min. The column temperature was kept at room temperature and the injection volume was 10 μl. Nitrogen was used as the nebulizer gas (GS1), heater gas (GS2), and curtain gas with the optimum values set at 35, 45 and 45 (arbitrary units), respectively. The source temperature was 450 °C and the ion spray voltage set at 5000 V. Declustering potential value was set to 150 V.

4.2. Local electrophilicity (local EPI) calculations

Full geometry optimizations and frequency analyses of DFT calculations were carried out in implicit aqueous solution at the B3LYP/6−311++G(2d,2p) level of theory using the Gaussian 09 program package [62]. Chemical descriptors were calculated from the optimized structures as described in the literature [43,63].

4.3. GSH reactivity assay

For thiol reactivity determination recently published assay was applied [41,44].

4.4. Oligopeptide selectivity assay

For residue selectivity determination, a recently puplished nonapeptide assay was applied [44].

4.5. Kinase activity assays

Fragments **1**−**24** were tested at 100 μM in duplicate data points with the Z′-LYTE kinase inhibition assay (Life Technologies). The assay employs a fluorescence-based format and is based on the different sensitivity of phosphorylated and non-phosphorylated peptides to proteolytic cleavage. A suitable peptide substrate is labeled with two fluorophores, forming a FRET pair. After 1 h preincubation with the test compounds the peptide substrate is added and incubating the kinase + peptide + test compound mixture for an additional hour, a development reaction is carried out. Any peptide that was not phosphorylated by the kinase is cleaved, disrupting the resonance energy transfer between the FRET pair. The reaction progress is quantified based on the ratio of the detected emission at 445 nm (coumarin) and 520 nm (fluorescein), *i.e.* the ratio of cleaved vs intact peptide. More detailed description of the assay is available on the website of Life Technologies [64]. IC_{50} values for **30**-**32** compounds were determined from 10 points titration measurements after the same preincubation protocol described above using the SelectScreen™ Biochemical Kinase Profiling Service available at Life Technologies.

4.6. JAK3 proteomics MS/MS

To 50 μL of the 12 μM JAK3 stock solution in 20 mM Tris at pH 8.0 with 150 mM NaCl and 2 mM $MnCl_2$, 1 μL of the covalent probes were added from a 100 mM DMSO stock solution, then the mixture was incubated at room temperature for 120 min. After the labelling, the mixture was digested immediately. Briefly 40−50 μL of the sample and 10 μL 0.2% (w/v) RapiGest SF (Waters, Milford, USA) solution buffered with 50 mM ammonium bicarbonate were mixed (pH = 7.8) and 3.3 μL of 45 mM DTT in 100 mM NH_4HCO_3 were added and kept at 37.5 °C for 30 min. After cooling the sample to room temperature, 4.2 μL of 100 mM iodoacetamide in 100 mM NH_4HCO_3 were added and placed in the dark in room temperature for 30 min. The reduced and alkylated protein was then digested by 10 μL (1 mg/mL) trypsin (the enzyme-to-protein ratio was 1: 10) (Sigma, St Louis, MO, USA). The sample was incubated at 37 °C for overnight. To degrade the surfactant, 7 μL of formic acid (500 mM) solution was added to the digested JAK3 sample and it was incubated at 37 °C for 45 min. For LC-MS analysis, the acid treated sample was centrifuged for 5 min at 13 000 rpm. QTRAP 6500 triple quadruple − linear ion trap mass spectrometer, equipped with a

Turbo V source in electrospray mode (AB Sciex, CA, USA) and a PerkinElmer Series 200 micro LC system (Massachusetts, USA) was used for LC-MS/MS analysis. Data acquisition and processing were performed using Analyst software version 1.6.2 (AB Sciex Instruments, CA, USA). Chromatographic separation was achieved by using the Vydac 218 TP52 Protein & Peptide C18 column (250 mm × 2.1 mm, 5 μm). The sample was eluted with a gradient of solvent A (0.1% formic acid in water) and solvent B (0.1% formic acid in ACN). The flow rate was set to 0.2 mL min^{-1}. The initial conditions for separation were 5% B for 7 min, followed by a linear gradient to 90% B by 53 min, from 60 to 63 min 90% B is retained; from 64 to 65 min back to the initial conditions with 5% eluent B retained to 70 min. The injection volume was 10 μL (300 pmol on the column). Information Dependent Acquisiton (IDA) LC-MS/MS experiment was used to identify the modified tryptic JAK3 peptide fragments. Enhanced MS scan (EMS) was applied as survey scan and enhanced product ion (EPI) was the dependent scan. The collision energy in EPI experiments was set to rolling collision energy mode, where the actual value was set on the basis of the mass and charge state of the selected ion. Further IDA criteria: ions greater than: 400.000 m/z, which exceeds 106 counts, exclude former target ions for 30 s after 2 occurrences. In EMS and in EPI mode the scan rate was 1000 Da/s as well. Nitrogen was used as the nebulizer gas (GS1), heater gas (GS2), and curtain gas with the optimum values set at 50, 40 and 40 (arbitrary units). The source temperature was 350 °C and the ion spray voltage set at 5000 V. Declustering potential value was set to 150 V. GPMAW 4.2. software and ProteinProspector (http://prospector.ucsf.edu/prospector/mshome.htm) was used to analyze the large number of MS/MS spectra and identify the modified tryptic JAK3 peptides.

4.7. NMR measurements for MELK

The MELK protein and the ligands were dissolved in a 10% (v/v) D_2O and H_2O mixture containing 20 mM Tris buffer (pH 7.6), 150 mM NaCl and 10% glycerine. For the ^{19}F measurements, the MELK and the BTF ligands concentrations were 20 and 40 μM, respectively. As a reference, ^{19}F experiments were also performed without the target, containing the ligand species alone. All ^{19}F NMR spectra were recorded in the range of F −100 to 0 ppm. A delay time (D1) of 1 s was adopted. To maximize sensitivity, 256 scans were collected into 131072 data points. The Bruker pulse program, zg, was used with a receiver gain (RG) of 54. All ^{19}F NMR spectra were phased and baseline corrected using the Topspin 4.2 software package (Bruker BioSpin, Rheinstetten, Germany).

4.8. Covalent docking

The binding mode of compound **30** in the binding site of MELK (PDB structure 5IH9 [65]) was modeled with the Covdock workflow of the Schrödinger Suite in the more precise Pose Prediction mode [66]. Briefly, the workflow consists of (i) non-covalent docking to the binding site with Glide [67], (ii) formation of the covalent bond between the ligand and the reactive residue, if the geometry of the non-covalent binding pose permits, (iii) minimization of the resulting covalent complex with Prime [68], and (iv) re-scoring the minimized complex with Glide. Five poses were saved and visually assessed both for Cys70 and for Cys89, with the one in Fig. 5D proposed as the most plausible binding mode (based on the favorable H-bonding pattern and closeness of the core scaffold to the hinge region).

4.9. Synthesis

4.9.1. General procedure of Suzuki coupling [52]

To a solution of 4-chloro-7*H*-pyrrolo[2,3-*d*]pyrimidine (1 eq.) and boronic acid (1.3 eq.) in dioxane/H_2O (5:1), K_2CO_3 (3 eq.) and $Pd(PPh_3)_4$ (0,1 eq.) were added under Ar. The mixture was heated to 110 °C for 16 h. The mixture was concentrated and water and DCM were added. The resulting mixture was filtered and the filtrate extracted with CH_2Cl_2 (3 ×). The organic layer dried over anhydrous Na_2SO_4. The solvent was removed and the crude material purified by reverse phase chromatography (H_2O/CH_3CN = 10−100%).

4.9.2. 3-(7H-Pyrrolo[2,3-d]pyrimidin-4-yl)benzaldehyde (25)

4-Chloro-7*H*-pyrrolo[2,3-*d*]pyrimidine (**27**) (1.5 g; 9.76 mmol), (3-formylphenyl)boronic acid (**28**) (1.74 g; 11.7 mmol), K_2CO_3 (4.1 g; 29.4 mmol), $Pd(PPh_3)_4$ (1.25 g; 0.97 mmol) in dioxane/H_2O (5:1) 54 ml, 1.27 g (58%) yellow solid was obtained [1]. ^1H NMR (500 MHz, DMSO-d_6) δ 12.33 (s, 1H, NH), 10.17 (s, 1H, CHO), 8.89 (s, 1H, ArH), 8.70 (s, 1H, ArH), 8.50 (d, *J* = 7.7 Hz, 1H, ArH), 8.06 (d, *J* = 7.6 Hz, 1H, ArH), 7.81 (t, *J* = 7.7 Hz, 1H, ArH), 7.71 (d, *J* = 1.6 Hz, 1H, ArH), 6.96 (d, *J* = 3.2 Hz, 1H, ArH) ppm. ^{13}C NMR (126 MHz DMSO-d_6) δ 193.62, 154.49, 153.21, 151.35, 139.19, 137.16, 134.61, 130.60, 130.28, 130.24, 128.66, 115.03, 100.22 ppm. HRMS (ESI): $(M + H)^+$ calcd. for $C_{13}H_9N_3O^+$, 224.0823; found, 224.0819.

4.9.3. 3-(7H-Pyrrolo[2,3-d]pyrimidin-4-yl)aniline (26) [52]

To a solution of 4-chloro-7*H*-pyrrolo[2,3-*d*]pyrimidine (**27**) (1.5 g, 9.76 mmol) and (3-aminophenyl)boronic acid (**29**) (1.8 g, 11.7 mmol) in 54 mL dioxane/H_2O (5:1), K_2CO_3 (4.1 g, 29.4 mmol) and $Pd(PPh_3)_4$ (1.125 g, 0.97 mmol) were added under Ar. The mixture was heated to 110 °C for 16 h. The mixture was concentrated and water and DCM were added. The resulting mixture was filtered and the filtrate extracted with CH_2Cl_2 (3 ×). The organic layer was dried over anhydrous Na_2SO_4. The solvent was removed and the crude material purified by reverse phase chromatography (H_2O/CH_3CN = 10−100%). 610 mg (30%) yellow solid was obtained. ^1H NMR (500 MHz, DMSO-d_6) δ 13.06 (s, 1H, NH), 9.02 (s, 1H, ArH), 8.11 (s, 1H), 8.05 (d, *J* = 7.8 Hz, 1H, ArH), 7.93 (d, *J* = 2.7 Hz, 1H, ArH), 7.70 (t, *J* = 7.9 Hz, 1H, ArH), 7.56 (d, *J* = 8.0 Hz, 1H, ArH), 7.14 (d, *J* = 3.5 Hz, 1H, ArH) ppm.

4.9.4. 3-(3-(7H-Pyrrolo[2,3-d]pyrimidin-4-yl)phenyl)-2-cyanoacrylamide (30)

3-(7*H*-Pyrrolo[2,3-*d*]pyrimidin-4-yl)benzaldehyde (**25**) (223 mg, 1.0 mmol) and 2-cyanoacetamide (**35**) (126 mg, 1.5 mmol) were dissolved in methanol (10 mL). Catalytic NaOH (1 mg, 1%) was added, and the reaction was stirred at 45 °C for 4 h. The reaction was concentrated under vacuum. The residue was purified on reversed phase column chromatography with a mixture of water and acetonitrile as eluent. The product was obtained as colorless oil (58 mg, 20%). ^1H NMR (500 MHz, DMSO-d_6) δ 12.32 (s, 1H, NH), 8.85 (s, 1H, ArH), 8.70 (s, 1H, ArH), 8.36 (d, *J* = 7.8 Hz, 1H, ArH), 8.33 (s, 1H, −CH =), 8.06 (d, *J* = 7.6 Hz, 1H, ArH), 7.95 (s, 1H, C(O)NH_2), 7.76 (m, 2H, ArH and C(O)NH_2), 7.68 (d, *J* = 3.3 Hz, 1H, ArH), 7.01 (d, *J* = 3.3 Hz, 1H, ArH) ppm. ^{13}C NMR (125 MHz, DMSO-d_6) δ 172.48, 163.17, 154.63, 153.18, 150.75, 139.21, 133.00, 132.54, 131.80, 130.28, 130.07, 128.57, 116.84, 115.00, 107.99, 100.26 ppm. HRMS (ESI): $(M + H)^+$ calcd. for $C_{16}H_{11}N_5O^+$, 290.1041; found, 290.1039.

4.9.5. N-(3-(7H-Pyrrolo[2,3-d]pyrimidin-4-yl)phenyl)-2-bromopropanamide (31)

To a solution of 3-(7*H*-pyrrolo[2,3-*d*]pyrimidin-4-yl)aniline (**26**) (210 mg; 1.0 mmol) in 3 ml DCM at 0 °C TEA (417 μl; 3.0 mmol) was added followed by the dropwise addition of 2-bromopropanoil chloride (**36**) (111 μl; 1.1 mmol). After addition, the mixture was stirred at room temperature for 1 h. The solvent was removed, and the crude material purified by flash chromatography (CH_2Cl_2/MeOH = 1–5%) to give 175 mg (50%) product as yellow solid. ^{1}H NMR (500 MHz, DMSO-d_6) δ 12.28 (s, 1H, NH), 10.55 (s, 1H, C(O)NH), 8.84 (s, 1H, ArH), 8.57 (s, 1H, ArH), 7.94 (d, $J = 7.6$ Hz, 1H, ArH), 7.75 (d, $J = 7.3$ Hz, 1H, ArH), 7.70 (s, 1H, ArH), 7.56 (d, $J = 7.9$ Hz, 1H, ArH), 6.95 (s, 1H, ArH), 4.79–4.68 (m, 1H, CHBr), 1.80 (d, $J = 6.6$ Hz, 2H, CH_3), 1.66 (d, $J = 6.6$ Hz, 1H, CH_3) ^{13}C NMR (125 MHz, DMSO-d_6) δ 168.21, 155.20, 153.15, 151.07, 139.43, 139.34, 129.85, 128.47, 124.28, 121.23, 119.95, 114.90, 100.46, 44.90, 21.83 ppm. HRMS (ESI): $(M + H)^+$ calcd. for $C_{15}H_{13}BrN_4O^+$, 345.0350; found, 345.0348.

4.9.6. N-(3-(7H-Pyrrolo[2,3-d]pyrimidin-4-yl)phenyl)acetamide (32)

3-(7*H*-pyrrolo[2,3-*d*]pyrimidin-4-yl)aniline (**26**) (210 mg, 1.0 mmol) was stirred under Ar atmosphere in 5 mL acetic anhydride (**37**) at RT overnight. The reaction mixture was concentrated under vacuum and the crude product was further purified on reversed phase column chromatography with a mixture of water and acetonitrile as eluent. Finally, **32** was obtained as black powder (43 mg, 17%). ^{1}H NMR (500 MHz, DMSO-d_6) δ 12.22 (s, 1H, NH), 10.13 (s, 1H, C(O)NH), 8.81 (s, 1H, ArH), 8.50 (s, 1H, ArH), 7.85 (d, $J = 7.8$ Hz, 1H, ArH), 7.72 (d, $J = 8.1$ Hz, 1H, ArH), 7.65 (d, $J = 2.2$ Hz, 1H, ArH), 7.48 (t, $J = 7.9$ Hz, 1H, ArH), 6.91 (d, $J = 2.7$ Hz, 1H, ArH), 2.08 (s, 3H, CH_3) ppm. ^{13}C NMR (500 MHz, DMSO-d_6) δ 168.99, 155.66, 153.09, 151.25, 140.10, 138.69, 129.59, 128.12, 123.46, 120.82, 119.62, 114.89, 100.42, 24.50 ppm. HRMS (ESI): $(M + H)^+$ calcd. for $C_{14}H_{12}N_4O^+$, 253.1089; found, 253.1085.

Author contributions

L.P. and A.E. synthesized electrophilic fragments and covalent inhibitors. L.P. performed the theoretical calculations, the GSH assay, the nonapeptide assay, the JAK3 labelling experiments and wrote the manuscript in part. D.B was involved in computational studies and corresponding data analysis and wrote the manuscript in part. T.I. performed the oligopeptide assay analysis and the JAK3 proteomics MS/MS measurements. A.H. and T.M. performed the NMR measurements for MELK. P.Á.B. designed and supervised the syntheses and wrote the manuscript in part. G.M.K conceived and supervised the project, analyzed and interpreted data, and wrote the manuscript.

Declaration of competing interest

The authors declare that they have no known competing financial interests or personal relationships that could have appeared to influence the work reported in this paper.

Acknowledgement

This work was supported by the National Research, Development and Innovation Office of Hungary (NKFIH grant number K116904). P. Ábrányi-Balogh was supported by the postdoctoral fellowship of the Hungarian Science Foundation OTKA (PD124598) grant. The work of D. Bajusz is supported by the János Bolyai Research Scholarship of the Hungarian Academy of Sciences. The authors are grateful to Balázs Merő (RCNS) for the expression of MELK, Zoltán Kele (SZTE) for his contribution to the MS investigation of MELK protein, György G. Ferenczy (RCNS) and Greg Makara (ChemPass) for useful discussions on the manuscript.

Appendix A. Supplementary data

Supplementary data to this article can be found online at https://doi.org/10.1016/j.ejmech.2020.112836.

References

[1] R.A. Bauer, Covalent inhibitors in drug discovery: from accidental discoveries to avoided liabilities and designed therapies, Drug Discov. Today 20 (9) (2015) 1061–1073, https://doi.org/10.1016/j.drudis.2015.05.005.
[2] A. Abdeldayem, Y.S. Raouf, S.N. Constantinescu, R. Moriggl, P.T. Gunning, Advances in covalent kinase inhibitors, Chem. Soc. Rev. (2020), https://doi.org/10.1039/C9CS00720B.
[3] V.A. Miller, V. Hirsh, J. Cadranel, Y.-M. Chen, K. Park, S.-W. Kim, C. Zhou, W.-C. Su, M. Wang, Y. Sun, et al., Afatinib versus placebo for patients with advanced, metastatic non-small-cell lung cancer after failure of erlotinib, gefitinib, or both, and one or two lines of chemotherapy (LUX-Lung 1): a phase 2b/3 randomised trial, Lancet Oncol. 13 (5) (2012) 528–538, https://doi.org/10.1016/S1470-2045(12)70087-6.
[4] P. Cohen, The origins of protein phosphorylation, Nat. Cell Biol. 4 (5) (2002) E127–E130, https://doi.org/10.1038/ncb0502-e127.
[5] S.K. Grant, Therapeutic protein kinase inhibitors, Cell. Mol. Life Sci. 66 (7) (2009) 1163–1177, https://doi.org/10.1007/s00018-008-8539-7.
[6] H. Gharwan, H. Groninger, Kinase inhibitors and monoclonal antibodies in oncology: clinical implications, Nat. Rev. Clin. Oncol. 13 (4) (2016) 209–227, https://doi.org/10.1038/nrclinonc.2015.213.
[7] R. Santos, O. Ursu, A. Gaulton, A.P. Bento, R.S. Donadi, C.G. Bologa, A. Karlsson, B. Al-Lazikani, A. Hersey, T.I. Oprea, et al., A comprehensive map of molecular drug targets, Nat. Rev. Drug Discov. 16 (1) (2017) 19–34, https://doi.org/10.1038/nrd.2016.230.
[8] Z. Zhao, P.E. Bourne, Progress with covalent small-molecule kinase inhibitors, Drug Discov. Today 23 (3) (2018) 727–735, https://doi.org/10.1016/j.drudis.2018.01.035.
[9] A. Yver, Osimertinib (AZD9291)—a science-driven, collaborative approach to rapid drug design and development, Ann. Oncol. 27 (6) (2016) 1165–1170, https://doi.org/10.1093/annonc/mdw129.
[10] Z.A. Knight, H. Lin, K.M. Shokat, Targeting the cancer kinome through polypharmacology, Nat. Rev. Canc. 10 (2) (2010) 130–137, https://doi.org/10.1038/nrc2787.
[11] C. Brzezniak, C.A. Carter, G. Giaccone, Dacomitinib, a new therapy for the treatment of non-small cell lung cancer, Expet Opin. Pharmacother. 14 (2) (2013) 247–253, https://doi.org/10.1517/14656566.2013.758714.
[12] J. Wu, M. Zhang, D. Liu, Acalabrutinib (ACP-196): a selective second-generation BTK inhibitor, J. Hematol. Oncol. 9 (1) (2016) 21, https://doi.org/10.1186/s13045-016-0250-9.
[13] Z. Pan, H. Scheerens, S.-J. Li, B.E. Schultz, P.A. Sprengeler, L.C. Burrill, R.V. Mendonca, M.D. Sweeney, K.C.K. Scott, P.G. Grothaus, et al., Discovery of selective irreversible inhibitors for Bruton's tyrosine kinase, ChemMedChem 2 (1) (2007) 58–61, https://doi.org/10.1002/cmdc.200600221.
[14] T.A. Baillie, Targeted covalent inhibitors for drug design, Angew. Chem. Int. Ed. 55 (43) (2016) 13408–13421, https://doi.org/10.1002/anie.201601091.
[15] D.A. Shannon, E. Weerapana, Covalent protein modification: the current landscape of residue-specific electrophiles, Curr. Opin. Chem. Biol. 24 (2015) 18–26, https://doi.org/10.1016/j.cbpa.2014.10.021.
[16] R. Lonsdale, J. Burgess, N. Colclough, N.L. Davies, E.M. Lenz, A.L. Orton, R.A. Ward, Expanding the armory: predicting and tuning covalent warhead reactivity, J. Chem. Inf. Model. 57 (12) (2017) 3124–3137, https://doi.org/10.1021/acs.jcim.7b00553.
[17] M. Gehringer, S.A. Laufer, Emerging and Re-emerging warheads for targeted covalent inhibitors: applications in medicinal chemistry and chemical biology, J. Med. Chem. 62 (12) (2019) 5673–5724, https://doi.org/10.1021/acs.jmedchem.8b01153.
[18] T. Zhang, J.M. Hatcher, M. Teng, N.S. Gray, M. Kostic, Recent advances in selective and irreversible covalent ligand development and validation, Cell. Chem. Biol. 26 (11) (2019) 1486–1500, https://doi.org/10.1016/j.chembiol.2019.09.012.
[19] J. Du, X. Yan, Z. Liu, L. Cui, P. Ding, X. Tan, X. Li, H. Zhou, Q. Gu, J. Xu, CBinderDB: a covalent binding agent database, Bioinformatics 33 (8) (2017) 1258–1260, https://doi.org/10.1093/bioinformatics/btw801.
[20] M. Gersch, J. Kreuzer, S.A. Sieber, Electrophilic natural products and their biological targets, Nat. Prod. Rep. 29 (6) (2012) 659–682, https://doi.org/10.1039/c2np20012k.
[21] L.M. McGregor, M.L. Jenkins, C. Kerwin, J.E. Burke, K.M. Shokat, Expanding the scope of electrophiles capable of targeting K-ras oncogenes, Biochemistry 56 (25) (2017) 3178–3183, https://doi.org/10.1021/acs.biochem.7b00271.
[22] E. Weerapana, C. Wang, G.M. Simon, F. Richter, S. Khare, M.B.D. Dillon, D.A. Bachovchin, K. Mowen, D. Baker, B.F. Cravatt, Quantitative reactivity profiling predicts functional cysteines in proteomes, Nature 468 (7325) (2010) 790–795, https://doi.org/10.1038/nature09472.
[23] K.M. Backus, Applications of reactive cysteine profiling, in: Current Topics in Microbiology and Immunology, Springer-Verlag, Berlin, Heidelberg, 2018, https://doi.org/10.1007/82_2018_120.
[24] S. Wang, Y. Tian, M. Wang, M. Wang, G. Sun, X. Sun, Advanced activity-based protein profiling application strategies for drug development, Front. Pharmacol. 9 (2018) 353, https://doi.org/10.3389/fphar.2018.00353.
[25] K. Shiraiwa, R. Cheng, H. Nonaka, T. Tamura, I. Hamachi, Chemical tools for endogenous protein labeling and profiling, Cell. Chem. Biol. 27 (8) (2020)

970–985, https://doi.org/10.1016/j.chembiol.2020.06.016.
[26] E. Awoonor-Williams, C.N. Rowley, How reactive are druggable cysteines in protein kinases? J. Chem. Inf. Model. 58 (9) (2018) 1935–1946, https://doi.org/10.1021/acs.jcim.8b00454.
[27] Z. Zhao, Q. Liu, S. Bliven, L. Xie, P.E. Bourne, Determining cysteines available for covalent inhibition across the human kinome, J. Med. Chem. 60 (7) (2017) 2879–2889, https://doi.org/10.1021/acs.jmedchem.6b01815.
[28] R. Liu, Z. Yue, C.-C. Tsai, J. Shen, Assessing lysine and cysteine reactivities for designing targeted covalent kinase inhibitors, J. Am. Chem. Soc. 141 (16) (2019) 6553–6560, https://doi.org/10.1021/jacs.8b13248.
[29] W. Zhang, J. Pei, L. Lai, Statistical analysis and prediction of covalent ligand targeted cysteine residues, J. Chem. Inf. Model. 57 (6) (2017) 1453–1460, https://doi.org/10.1021/acs.jcim.7b00163.
[30] J.S. Murray, P. Politzer, The electrostatic potential: an overview, Wiley Interdiscip. Rev. Comput. Mol. Sci. 1 (2) (2011) 153–163, https://doi.org/10.1002/wcms.19.
[31] G. Naray-Szabo, G.G. Ferenczy, Molecular electrostatics, Chem. Rev. 95 (4) (1995) 829–847, https://doi.org/10.1021/cr00036a002.
[32] M.S. Cohen, Structural bioinformatics-based design of selective, irreversible kinase inhibitors, Science 308 (80) (2005) 1318–1321, https://doi.org/10.1126/science1108367, 5726.
[33] E. Leproult, S. Barluenga, D. Moras, J.-M. Wurtz, N. Winssinger, Cysteine mapping in conformationally distinct kinase nucleotide binding sites: application to the design of selective covalent inhibitors, J. Med. Chem. 54 (5) (2011) 1347–1355, https://doi.org/10.1021/jm101396q.
[34] Q. Liu, Y. Sabnis, Z. Zhao, T. Zhang, S.J. Buhrlage, L.H. Jones, N.S. Gray, Developing irreversible inhibitors of the protein kinase cysteinome, Chem. Biol. 20 (2) (2013) 146–159, https://doi.org/10.1016/j.chembiol.2012.12.006.
[35] E. Awoonor-Williams, A.G. Walsh, C.N. Rowley, Modeling covalent-modifier drugs, Biochim. Biophys. Acta Protein Proteonomics 1865 (11) (2017) 1664–1675, https://doi.org/10.1016/j.bbapap.2017.05.009.
[36] D.A. Erlanson, S.W. Fesik, R.E. Hubbard, W. Jahnke, H. Jhoti, Twenty years on: the impact of fragments on drug discovery, Nat. Rev. Drug Discov. 15 (9) (2016) 605–619, https://doi.org/10.1038/nrd.2016.109.
[37] A. Keeley, L. Petri, P. Ábrányi-Balogh, G.M. Keserű, Covalent fragment libraries in drug discovery, Drug Discov. Today (2020), https://doi.org/10.1016/j.drudis.2020.03.016.
[38] E.H. Krenske, R.C. Petter, K.N. Houk, Kinetics and thermodynamics of reversible thiol additions to mono- and diactivated michael acceptors: implications for the design of drugs that bind covalently to cysteines, J. Org. Chem. 81 (23) (2016) 11726–11733, https://doi.org/10.1021/acs.joc.6b02188.
[39] M.E. Flanagan, J.A. Abramite, D.P. Anderson, A. Aulabaugh, U.P. Dahal, A.M. Gilbert, C. Li, J. Montgomery, S.R. Oppenheimer, T. Ryder, et al., Chemical and computational methods for the characterization of covalent reactive groups for the prospective design of irreversible inhibitors, J. Med. Chem. 57 (23) (2014) 10072–10079, https://doi.org/10.1021/jm501412a.
[40] V.J. Cee, L.P. Volak, Y. Chen, M.D. Bartberger, C. Tegley, T. Arvedson, J. McCarter, A.S. Tasker, C. Fotsch, Systematic study of the glutathione (GSH) reactivity of N -arylacrylamides: 1. Effects of aryl substitution, J. Med. Chem. 58 (23) (2015) 9171–9178, https://doi.org/10.1021/acs.jmedchem.5b01018.
[41] L. Petri, P. Ábrányi-Balogh, P.R. Varga, T. Imre, G.M. Keserű, Comparative reactivity analysis of small-molecule thiol surrogates, Bioorg. Med. Chem. 28 (7) (2020) 115357, https://doi.org/10.1016/j.bmc.2020.115357.
[42] G.G. Ferenczy, G.M. Keserű, Thermodynamics of fragment binding, J. Chem. Inf. Model. 52 (4) (2012) 1039–1045, https://doi.org/10.1021/ci200608b.
[43] P.K. Chattaraj, U. Sarkar, D.R. Roy, Electrophilicity index, Chem. Rev. 106 (6) (2006) 2065–2091, https://doi.org/10.1021/cr040109f.
[44] P. Ábrányi-Balogh, L. Petri, T. Imre, P. Szijj, A. Scarpino, M. Hrast, A. Mitrović, U.P. Fonovič, K. Németh, H. Barreteau, et al., A road map for prioritizing warheads for cysteine targeting covalent inhibitors, Eur. J. Med. Chem. 160 (2018) 94–107, https://doi.org/10.1016/j.ejmech.2018.10.010.
[45] G. Manning, The protein kinase complement of the human genome, Science 298 (80) (2002) 1912–1934, https://doi.org/10.1126/science.1075762, 5600.
[46] M. Chartier, T. Chénard, J. Barker, R. Najmanovich, Kinome Render, A standalone and web-accessible tool to annotate the human protein kinome tree, PeerJ 1 (2013) e126, https://doi.org/10.7717/peerj.126.
[47] A. Vasudevan, M.A. Argiriadi, A. Baranczak, M.M. Friedman, J. Gavrilyuk, A.D. Hobson, J.J. Hulce, S. Osman, N.S. Wilson, Covalent binders in drug discovery, in: Progress in Medicinal Chemistry, 2019, https://doi.org/10.1016/bs.pmch.2018.12.002.
[48] E.R. Goedken, M.A. Argiriadi, D.L. Banach, B.A. Fiamengo, S.E. Foley, K.E. Frank, J.S. George, C.M. Harris, A.D. Hobson, D.C. Ihle, et al., Tricyclic covalent inhibitors selectively target Jak3 through an active site thiol, J. Biol. Chem. 290 (8) (2015) 4573–4589, https://doi.org/10.1074/jbc.M114.595181.
[49] L. Tan, K. Akahane, R. McNally, K.M.S.E. Reyskens, S.B. Ficarro, S. Liu, G.S. Herter-Sprie, S. Koyama, M.J. Pattison, K. Labella, et al., Development of selective covalent Janus kinase 3 inhibitors, J. Med. Chem. 58 (16) (2015) 6589–6606, https://doi.org/10.1021/acs.jmedchem.5b00710.
[50] J. Kempson, D. Ovalle, J. Guo, S.T. Wrobleski, S. Lin, S.H. Spergel, J.J.-W. Duan, B. Jiang, Z. Lu, J. Das, et al., Discovery of highly potent, selective, covalent inhibitors of JAK3, Bioorg. Med. Chem. Lett 27 (20) (2017) 4622–4625, https://doi.org/10.1016/j.bmcl.2017.09.023.
[51] J.-B. Telliez, M.E. Dowty, L. Wang, J. Jussif, T. Lin, L. Li, E. Moy, P. Balbo, W. Li, Y. Zhao, et al., Discovery of a JAK3-selective inhibitor: functional differentiation of JAK3-selective inhibition over pan-JAK or JAK1-selective inhibition, ACS Chem. Biol. 11 (12) (2016) 3442–3451, https://doi.org/10.1021/acschembio.6b00677.
[52] A. Thorarensen, M.E. Dowty, M.E. Banker, B. Juba, J. Jussif, T. Lin, F. Vincent, R.M. Czerwinski, A. Casimiro-Garcia, R. Unwalla, et al., Design of a Janus kinase 3 (JAK3) specific inhibitor 1-((2 S ,5 R)-5-((7 H -Pyrrolo[2,3- d]Pyrimidin-4-Yl)Amino)-2-Methylpiperidin-1-Yl)Prop-2-En-1-One (PF-06651600) allowing for the interrogation of JAK3 signaling in humans, J. Med. Chem. 60 (5) (2017) 1971–1993, https://doi.org/10.1021/acs.jmedchem.6b01694.
[53] M. Forster, M. Gehringer, S.A. Laufer, Recent advances in JAK3 inhibition: isoform selectivity by covalent cysteine targeting, Bioorg. Med. Chem. Lett 27 (18) (2017) 4229–4237, https://doi.org/10.1016/j.bmcl.2017.07.079.
[54] L. He, M. Shao, T. Wang, T. Lan, C. Zhang, L. Chen, Design, synthesis, and SAR study of highly potent, selective, irreversible covalent JAK3 inhibitors, Mol. Divers. 22 (2) (2018) 343–358, https://doi.org/10.1007/s11030-017-9803-2.
[55] R. Gunasekar, P. Thamaraiselvi, R.S. Rathore, K.I. Sathiyanarayanan, S. Easwaramoorthi, Tuning the electronic properties of 2-cyano-3-phenylacrylamide derivatives, J. Org. Chem. 80 (24) (2015) 12351–12358, https://doi.org/10.1021/acs.joc.5b02226.
[56] N. London, R.M. Miller, S. Krishnan, K. Uchida, J.J. Irwin, O. Eidam, L. Gibold, P. Cimermančič, R. Bonnet, B.K. Shoichet, et al., Covalent docking of large libraries for the discovery of chemical probes, Nat. Chem. Biol. 10 (12) (2014) 1066–1072, https://doi.org/10.1038/nchembio.1666.
[57] L. Ren, B. Deng, V. Saloura, J. Park, Y. Nakamura, MELK inhibition targets cancer stem cells through downregulation of SOX2 expression in head and neck cancer cells, Oncol. Rep. (2019), https://doi.org/10.3892/or.2019.6988.
[58] A. Chlenski, C. Park, M. Dobratic, H.R. Salwen, B. Budke, J.-H. Park, R. Miller, M.A. Applebaum, E. Wilkinson, Y. Nakamura, et al., Maternal embryonic leucine zipper kinase (MELK), a potential therapeutic target for neuroblastoma, Mol. Canc. Therapeut. 18 (3) (2019) 507–516, https://doi.org/10.1158/1535-7163.MCT-18-0819.
[59] A. Cigliano, M.G. Pilo, M. Mela, S. Ribback, F. Dombrowski, G.M. Pes, A. Cossu, M. Evert, D.F. Calvisi, K. Utpatel, Inhibition of MELK protooncogene as an innovative treatment for intrahepatic cholangiocarcinoma, Medicina (B Aires) 56 (1) (2019) 1, https://doi.org/10.3390/medicina56010001.
[60] M.H. Meel, M. Guillén Navarro, M.C. de Gooijer, D.S. Metselaar, P. Waranecki, M. Breur, T. Lagerweij, L.E. Wedekind, J. Koster, M.D. van de Wetering, et al., MEK/MELK inhibition and blood–brain barrier deficiencies in atypical teratoid/rhabdoid tumors, Neuro Oncol. 22 (1) (2020) 58–69, https://doi.org/10.1093/neuonc/noz151.
[61] I.M. McDonald, G.D. Grant, M.P. East, T.S.K. Gilbert, E.M. Wilkerson, D. Goldfarb, J. Beri, L.E. Herring, C. Vaziri, J.G. Cook, et al., Mass spectrometry–based selectivity profiling identifies a highly selective inhibitor of the kinase MELK that delays mitotic entry in cancer cells, J. Biol. Chem. 295 (8) (2020) 2359–2374, https://doi.org/10.1074/jbc.RA119.011083.
[62] M.J. Frisch, H.B. Schlegel, G.E. Scuseria, et al., Gaussian 09 (Revision A.02), Gaussian Inc, Wallingford, CT, 2009.
[63] D. Wondrousch, A. Böhme, D. Thaens, N. Ost, G. Schüürmann, Local electrophilicity predicts the toxicity-relevant reactivity of michael acceptors, J. Phys. Chem. Lett. 1 (10) (2010) 1605–1610, https://doi.org/10.1021/jz100247x.
[64] Z'-LYTE biochemical kinase assays. http://www.thermofisher.com/hu/en/home/industrial/pharma-biopharma/drug-discovery-development/target-and-lead-identification-and-validation/kinasebiology/kinase-activity-assays.html.
[65] B.B. Touré, J. Giraldes, T. Smith, E.R. Sprague, Y. Wang, S. Mathieu, Z. Chen, Y. Mishina, Y. Feng, Y. Yan-Neale, et al., Toward the validation of maternal embryonic leucine zipper kinase: discovery, optimization of highly potent and selective inhibitors, and preliminary biology insight, J. Med. Chem. 59 (10) (2016) 4711–4723, https://doi.org/10.1021/acs.jmedchem.6b00052.
[66] K. Zhu, K.W. Borrelli, J.R. Greenwood, T. Day, R. Abel, R.S. Farid, E. Harder, Docking covalent inhibitors: a parameter free approach to pose prediction and scoring, J. Chem. Inf. Model. 54 (7) (2014) 1932–1940, https://doi.org/10.1021/ci500118s.
[67] R.A. Friesner, J.L. Banks, R.B. Murphy, T.A. Halgren, J.J. Klicic, D.T. Mainz, M.P. Repasky, E.H. Knoll, M. Shelley, J.K. Perry, et al., Glide: a new approach for rapid, accurate docking and scoring. 1. Method and assessment of docking accuracy, J. Med. Chem. 47 (7) (2004) 1739–1749, https://doi.org/10.1021/jm0306430.
[68] M.P. Jacobson, D.L. Pincus, C.S. Rapp, T.J.F. Day, B. Honig, D.E. Shaw, R.A. Friesner, A hierarchical approach to all-atom protein loop prediction, Proteins Struct. Funct. Bioinforma. 55 (2) (2004) 351–367, https://doi.org/10.1002/prot.10613.